HHS Public Access

Author manuscript

Cancer Res. Author manuscript; available in PMC 2021 October 15.

Published in final edited form as:

Cancer Res. 2021 April 15; 81(8): 2086–2100. doi:10.1158/0008-5472.CAN-20-2218.

Therapeutic targeting of DGKA-mediated macropinocytosis leads to phospholipid reprogramming in Tuberous Sclerosis Complex

Andrii Kovalenko[1], **Andres Sanin**[1], **Kosmas Kosmas**[1], **Long Zhang**[1], **Ji Wang**[1], **Elie W. Akl**[1], **Krinio Giannikou**[1], **Clemens K. Probst**[1], **Thomas R. Hougard**[1], **Ryan W. Rue**[2], **Vera P. Krymskaya**[2], **John M. Asara**[3], **Hilaire C. Lam**[1], **David J. Kwiatkowski**[1], **Elizabeth P. Henske**[1,*], **Harilaos Filippakis**[1,*]

[1]Pulmonary and Critical Care Medicine, Brigham and Women's Hospital, Harvard Medical School, Boston, MA, USA

[2]Division of Pulmonary, Allergy and Critical Care Medicine, Department of Medicine, Lung Biology Institute, Perelman School of Medicine, University of Pennsylvania, PA, USA

[3]Division of Signal Transduction, Beth Israel Deaconess Medical Center, Department of Medicine, Harvard Medical School Boston, MA, USA

Abstract

Lymphangioleiomyomatosis (LAM) is a rare destructive lung disease affecting primarily women and is the primary lung manifestation of tuberous sclerosis complex (TSC). In LAM, biallelic loss of TSC1/2 leads to hyperactivation of mTORC1 and inhibition of autophagy. To determine how the metabolic vulnerabilities of TSC2-deficient cells can be targeted, we performed a high throughput screen utilizing the "Repurposing" library at the Broad Institute, with or without the autophagy inhibitor chloroquine. Ritanserin, an inhibitor of diacylglycerol kinase alpha (DGKA), was identified as a selective inhibitor of proliferation of $Tsc2^{-/-}$ MEFs, with no impact on $Tsc2^{+/+}$ MEFs. DGKA is a lipid kinase that metabolizes diacylglycerol (DAG) to phosphatidic acid (PA), a key component of plasma membranes. PA levels were increased 5-fold in $Tsc2^{-/-}$ MEFs compared to $Tsc2^{+/+}$ MEFs, and treatment of $Tsc2^{-/-}$ MEFs with ritanserin led to depletion of PA as well as rewiring of phospholipid metabolism. Macropinocytosis is known to be upregulated in TSC2-deficient cells. Ritanserin decreased macropinocytic uptake of albumin, limited the number of lysosomes, and reduced lysosomal activity in $Tsc2^{-/-}$ MEFs. In a mouse model of TSC, ritanserin treatment decreased cyst frequency and volume, and in a mouse model of LAM, genetic downregulation of DGKA prevented alveolar destruction and airspace enlargement. Collectively, these data indicate that DGKA supports macropinocytosis in TSC2-deficient cells to maintain phospholipid homeostasis and promote proliferation. Targeting macropinocytosis with ritanserin may represent a novel therapeutic approach for the treatment of TSC and LAM.

[*]**Corresponding authors:** Harilaos Filippakis, Brigham and Women's Hospital, Department of Medicine, Pulmonary and Critical Care Medicine, TH-8-826A, Boston, Massachusetts, USA, Phone: +1 857-307-0794, cfilippakis@bwh.harvard.edu, Elizabeth P. Henske, Brigham and Women's Hospital, Department of Medicine, Pulmonary and Critical Care Medicine, TH-8-826B, Boston, Massachusetts, USA, Phone: +1 857-307-0782, ehenske@bwh.harvard.edu.

Conflict of Interest: The authors declare no potential conflicts of interest.

Keywords

Tuberous Sclerosis Complex; Lymphangioleiomyomatosis; mTORC1; macropinocytosis; phospholipid metabolism; DGKA

INTRODUCTION

Tuberous Sclerosis Complex (TSC) is an autosomal dominant genetic disease that affects multiple organ systems including the brain, kidney, heart, skin, and lung[1,2]. In the lung, TSC manifests as lymphangioleiomyomatosis (LAM), which is characterized by neoplastic growth of tumors (LAM nodules) and cyst formation in the airways leading to lung destruction, pneumothorax and chylous pleural effusion[3,4]. LAM arises primarily in women and progresses more rapidly in premenopausal women than in postmenopausal women and occurs in up to 80% of women with TSC[5]. Importantly, LAM can also occur in women who do not have TSC (sporadic LAM). Sporadic and TSC-associated LAM lesions exhibit loss of function mutations in *TSC2*, followed by loss of heterozygosity leading to complete loss of *TSC2*[6,7]. Biallelic loss of *TSC1/2* leads to hyperactivation of the mechanistic/mammalian target of rapamycin complex 1 (mTORC1), a master regulator of anabolic cell growth and metabolism[8,9]. mTORC1-driven metabolic reprogramming in TSC leads to increased uptake and utilization of extracellular nutrients, including glucose and glutamine, creating metabolic dependencies that can be therapeutically targeted[10]. We have previously found that targeting the nutrient uptake pathway of macropinocytosis and lysosomal processing in TSC2-deficient cells may provide novel therapeutic approaches in TSC and LAM[11,12].

Macropinocytosis is a conserved, actin-dependent endocytic process that allows the bulk uptake of extracellular fluids into large vesicles called macropinosomes[13–15]. In cancer metabolism studies, transformed cells exploit macropinocytosis to engulf and process macromolecules at the lysosome to fuel anabolic metabolism and support proliferation[16–18]. Lysosomes represent a central signaling hub, maintaining cellular metabolic homeostasis by recruiting and activating mTORC1. Furthermore, nutrient sensing at the lysosomal surface is coupled with mTORC1-dependent activation of its downstream targets[19].

Phospholipids are essential components of cellular membranes for structural, metabolic, and signaling pathway functions[20,21]. Their ability to undergo hydrolysis or head-group modifications confer plasticity to biological membranes[22]. Phospholipids play an important role in endocytic trafficking and in macropinocytosis, through their ability to organize and influence the polymerization and branching of filamentous actin (F-actin). Of note, diacylglycerol (DAG) and phosphatidic acid (PA), derived from the phospholipid PtdIns(4,5)P_2, drive macropinocytosis by initiating the formation of membrane ruffles and macropinosomes[23,24]. A critical step in the metabolism of PA from DAG is performed by diacylglycerol kinase alpha (DGKA), a lipid kinase that has been identified as a positive regulator of carcinogenesis[25,26]. Recently, DGKA activity has been found to be strongly inhibited by ritanserin, via a mechanism that involves binding to the catalytic site of DGKs[27,28]. Ritanserin was first identified as a serotonin receptor (5-HTR) antagonist and

has been used in clinical trials to treat schizophrenia and substance dependence[29–31], making it a potential repurposing drug for the treatment of DGKA-driven malignancies[32,33].

Here, we report the impact of ritanserin on TSC2-deficient cell phospholipid metabolism and identify DGKA as a critical node in macropinocytosis-mediated nutrient uptake. We found that exogenous protein uptake via macropinocytosis is mediated by DGKA, and that pharmacologic or genetic inhibition of DGKA leads to lipid reprogramming in TSC2-deficient cells. Importantly, the enhanced macropinocytosis observed in TSC2-deficient cells can be therapeutically targeted by the DGKA inhibitor ritanserin.

MATERIALS & METHODS

Cell lines and culture conditions

Littermate-derived $Tsc2^{-/-}$ $p53^{-/-}$ and $Tsc2^{+/+}$ $p53^{-/-}$ mouse embryonic fibroblasts (MEF) were used[34]. In addition, MEFs were isolated from Tsc2flox/flox-Rosa26-CreERT2 embryos and subclones were generated with knockout of Tsc2 (Tsc2 KO MEFs) as well as ethanol-treated controls (Tsc2 WT MEFs), as described previously[35]. 105K $Tsc2^{-/-}$ is a cell line derived from a $Tsc2^{+/-}$ C57Bl/6 mouse renal tumor and confirmed via to have a loss of the second Tsc2 allele, loss of Tsc2 expression, and hyperactive mTORC1[36]. 105K+Tsc2 and 105K+EV cells were generated by re-expressing Tsc2 in 105K cells using retroviral delivery of pLXIN-IRES-hygromycin vector carrying full-length human TSC2 or empty vector respectively[12]. TTJ cells were generated $Tsc2^{-/+}$ C57BL/6 mice, first in immunodeficient nude BALB/c mice and then in C57BL/6 mice[37]. The 621–101 cells are a TSC2-deficient human kidney angiomyolipoma-derived cell line, immortalized by introducing E6/E7 (pLXSN 16E6E7-neo) and human telomerase (pLXSN hTERT-hyg)[38]. The 621–103 are an addback cell line generated by transfection with the TSC2 cDNA. The sgAtg5 cells were generated from $Tsc2^{-/-}$ $p53^{-/-}$ and $Tsc2^{+/+}$ $p53^{-/-}$ MEFs as previously described[11]. Lentiviral vectors carrying DGKA shRNA were used to knock-down *DGKA* in $Tsc2^{+/+}$ $p53^{-/-}$ and $Tsc2^{-/-}$ $p53^{-/-}$ MEFs, 105K+TSC2, 105K+EV, and TTJ cells. Lentiviral constructs were obtained from Sigma Aldrich (DGKA#1: TRCN0000361167, DGKA#2: TRCN0000378505, DGKA#3: TRCN0000368765). Following viral transduction, pools of cells with stable shRNA expression were selected using puromycin (10ug/ml) and knockdown of DGKA was validated using RT-qPCR and immunoblotting. Unless specified otherwise, cells were cultured in Dulbecco's modified Eagle medium containing 4.5 g/l glucose supplemented with 10% FBS, 100ug/mL penicillin and 100ug/mL streptomycin. All cells tested negative for mycoplasma and were re-tested monthly using MycoAlert (Lonza, Walkerville, MD).

Antibodies, drugs and reagents

The following antibodies were used: Tsc2, pS6 ribosomal, S6 ribosomal protein, PARP, Cleaved Caspase 3, (Cell Signaling Technology), actin (Sigma-Aldrich). Rapamycin and Torin1 were purchased from LC Laboratories. Chloroquine and 5-(N-Ethyl-N-isopropyl) amiloride (EIPA) were purchased from Sigma-Aldrich. Ritanserin was purchased from Tocris (Cat. No. 1955). Phosphatidic acid was purchased from Avanti Polar Lipids.

High throughput drug screen

Screening of approximately 7,000 compounds from the Repurposing Hub were screened using the resources of the Chemical Biology Program of the Broad Institute of MIT and Harvard (https://clue.io/repurposing)[39]. 500 $Tsc2^{-/-}$ and $Tsc2^{+/+}$ MEFs treated with 5uM CQ or vehicle control (H_2O) were seeded in each well of a 384-well plate and allowed to attach overnight. On the following day, cells were treated in duplicate with 100nL of screening compounds (10uM) using a CyBio Well Vario (Analytikjena). Cell viability was assessed 48 hours later by adding Cell Titer Glo (Promega) at a 1:1 ratio and data were normalized to plate background variability using an Envision Multilabel Reader (PerkinElmer). Staurosporine (2uM) was used in each plate as a positive control.

Angiomyolipoma transcriptomic analysis

We performed whole transcriptome RNA-seq analysis in 18 kidney angiomyolipomas and 4 normal kidneys. The gene expression data from this cohort were integrated to data from 10 additional kidney angiomyolipomas and 4 normal kidneys, previously reported[40]. Briefly, total RNA was isolated using the RNeasy mini kit (Qiagen, Germany, Cat. No 34501). High quality of 1μgr mRNA (RIN>8; Agilent 2100 Bioanalyzer) was subject to cDNA library preparation using manufacturer's instructions (Illumina platform). DsDNA libraries were quantified by Qubit fluorometer, Agilent TapeStation 2200, and RT-qPCR using the Kapa Biosystems library quantification kit and then they were sequenced in HiSeq2500. A total of 2×75 bp paired end reads and ~50 million reads were generated for each sample. Sequence reads were aligned to the UCSC hg19 human genome build using the STAR aligning program [41]. Quantification of all genes and their isoforms was performed using FPKM normalized values by applying Cufflinks v2.2.1.

mRNA expression analysis

RNA extraction was performed using RNeasy Micro Kit (Qiagen Inc., Valencia, CA, USA). Two micrograms of total protein were retrotranscribed using the High-Capacity cDNA Reverse Transcription Kit (Applied Biosystems, Grand Island, NY, USA). Forty nanograms of cDNA were used for qPCR reactions, using TaqMan probes and TaqMan Fast Advanced Master Mix (Applied Biosystems) in an Applied Biosystems Instrument. The data was analyzed using the ΔΔCt method. Actin was used as a reference gene since it was expressed uniformly across tested groups.

Crystal violet staining

1500 cells per well were plated in 96-well plates and allowed to attach overnight. Drug treatments were administered on the following day. After incubation for 24, 48 or 72 hours, cells were fixed with 10% formalin for 10 minutes, stained with 0.05% (w/v) crystal violet in distilled water for 30 minutes, washed three times by submerging the plates in clean tap water and air dried. Crystal violet was solubilized by adding 100uL of methanol per well. The absorbance was measured with a plate reader (OD 540; BioTek, Winooski, VT, USA).

Macropinocytosis uptake assays and flow cytometry

Cells were seeded in 6-well plates and grown in 1% FBS DMEM overnight. Treatments with ritanserin (10uM) or EIPA (25uM) were carried out for 16 hours followed by addition of 0.5 mg/ml 70 kDa FITC-Dextran or BSA-TMR (Invitrogen, Carlsbad, CA, USA) for 1 hour as described previously[11]. Cells were subsequently washed twice with ice-cold PBS, trypsinized and recovered in 2% serum phenol red-free DMEM and centrifuged 425 × g for 2 minutes. The pelleted cells were resuspended in 300 ul of serum-free, phenol red-free DMEM and kept on ice. Fluorescence was assessed by flow cytometry (BD FACS Canto II, BD Biosciences), and analyzed with FlowJo analytical software (Treestar). Median fluorescence intensity of FITC (Dextran) or APC (BSA-TMR) were measured in each sample and values were normalized to those of Tsc2-expressing unstained cells.

DAG Kinase Assay

The DAG kinase assay protocol was adapted from procedures described previously[42]. Cells growing in 100mm cell culture dishes at 80% confluency were lysed on ice using the following lysis buffer: 50 mM HEPES, pH 7.2, 150 mM NaCl, 5 mM MgCl2, 1 mM dithiothreitol, 1 mM phosphatase inhibitor cocktail and 1mM protease inhibitor cocktail. After centrifugation at 400 g for 5 min, the resultant supernatant was used for the DAG Kinase activity assay. The enzymatic reactions were carried out in triplicate in 384-well white plates, in the final volume of 10uL, in the solution of the following final composition: 50 mM MOPS, pH 7.4, 50 mM n-octyl b-D-glucopyranose (Sigma-Aldrich), 1 mM dithiothreitol, 100 mM NaCl, 20 mM NaF, 10 mM $MgCl_2$, 1 mM $CaCl_2$, 10 mM phosphatidylserine (Sigma-Aldrich), 2 mM 1,2-dioleoyl-sn-glycerol (Sigma-Aldrich), 0.2 mM ATP. The enzymatic reactions were incubated at 37°C for 90 minutes. 10uL of ADP-Glo reagent (Promega) was added at 25°C. Following 40 minutes incubation, 20uL of Kinase Detection Reagent (Promega) was added. After additional 40 minutes of incubation at 25 °C, luminescence was detected using the BioTek plate reader (BioTek, Winooski, VT, USA) with sensitivity set to 100. ATP was used as a positive control and lysates heated at 70°C for 15 minutes (protein denaturing conditions) were used as a negative control.

Confocal microscopy

Cells were seeded on 4-chamber tissue culture glass slides using 1% FBS DMEM overnight. Cells were treated with inhibitors for 16 hours and BODIPY (493/503) and Phalloidin (578/600) were added for 30 minutes. Cells were then rinsed twice with PBS and fixed with 4% paraformaldehyde. Images were captured with a FluoView FV-10i Olympus Laser Point Scanning Confocal Microscope using a 60x objective. Confocal filters (Excitation/Emission nm) used for microscopy imaging were: 358/461 (DAPI), 494/521 (FITC-Dextran).

Steady state metabolite profiling and analysis

Metabolites from four replicate 60mm plates were extracted with 80% aqueous methanol. Metabolites were processed using Selected Reaction Monitoring (SRM) with polarity switching on a 5500 QTRAP triple quadrupole mass spectrometer (AB/SCIEX) coupled to a Prominence UFLC HPLC system (Shimadzu) using amide HILIC chromatography (Waters) at pH 9.2 (Metabolomics Core, Beth Israel Deaconess Medical Center, Boston, MA). Two

hundred fifty-two endogenous water-soluble metabolites were measured at steady state. Metabolomic peak area data were normalized to protein concentration of three additional replicate plates and uploaded into MetaboAnalyst 4.0 (http://www.metaboanalyst.ca/MetaboAnalyst/) for subsequent processing and metabolite set enrichment analysis. In detail, data were filtered by interquartile range and autoscaling was applied to normalize data by metabolite (mean-centered and divided by the standard deviation of each variable). Log2 transformation and statistical tests were applied. For two-group comparisons, t-test followed by False Discovery Rate correction was used. Two-way ANOVA test was applied for comparing multiple groups. Significance was defined with $q<0.05$ and $p<0.05$, respectively.

Lipidomic profiling

Lipid species were extracted from four replicate 60mm plates using MTBE/Methanol extraction and peak area vales were obtained using liquid chromatography mass spectrometry (LC-MS) as described previously (Metabolomics Core, Beth Israel Deaconess Medical Center, Boston, MA)[43]. Peak area values were normalized to three additional protein plates for each condition. Each lipid moiety is represented as the sum of individual lipid species +/− SD. For two-group comparisons, t-test followed by False Discovery Rate correction was used. Significance was defined with $p<0.05$.

Animal studies

All animal studies were performed in accordance with institutional protocols approved by the BWH Institutional Animal Care and Use Committee. Female NCr nude mice were purchased from Taconic and injected with 3 million TTJ cells stably expressing DGKA shRNA (DGKA#3: TRCN0000368765). The median linear intercept (MLI) of alveolar airspace from four images per mouse was calculated using ImageJ as previously described[44]. The ritanserin study was carried out at the Van Andel Institute (VAI) according to institutional protocols. 10 $Tsc2^{+/-}$ A/J mice ~7 months of age (5 males and 5 females) were randomly assigned to the vehicle (0.25% PEG200, 0.25% Tween-80 in water) or ritanserin (20mg/kg; TOCRIS #1955) treatment group. Mice were treated intraperitoneally for 30 days and euthanized 1 hour following final treatment. Kidneys were harvested and placed in 10% NBF for 24–72 hours. Each kidney was then split longitudinally in the middle and embedded into paraffin blocks. H&E staining was performed in 5um thick tissue sections and 3 sections per kidney were used for tumor scoring according to a previously established formula[45].

Statistical analyses

Normally distributed data were analyzed for statistical significance with Student's unpaired t-test and multiple comparisons were made with one-way and two-way ANOVAs with Bonferroni correction. In vivo data are presented as the mean +/− 95% confidence interval (CI) and in vitro studies are presented as the mean +/− standard deviation (SD). (GraphPad Prism version 7; GraphPad Software, www.graphpad.com).

Statistical significance was defined as $p < 0.05$.

RESULTS

Chloroquine synergizes with ritanserin to selectively inhibit the proliferation of TSC2-deficient cells

To search for therapeutic approaches selective against TSC2-deficient cells, we performed a high-throughput compound screen of ~7,000 FDA-approved and clinical trial drugs (see Methods). $Tsc2^{+/+}$ and $Tsc2^{-/-}$ MEFs were treated with either vehicle control (DMSO) or CQ (5uM). The potent inducer of apoptosis, Staurosporine (2uM) was used as a positive control. Sixteen hours later cells were treated with compounds from the library at a single common dose of 10uM for 48 hours. Twenty-two compounds that inhibited the proliferation of $Tsc2^{-/-}$ MEFs treated with CQ were identified. Compounds that had no effect on vehicle treated $Tsc2^{-/-}$ MEFs or $Tsc2^{+/+}$ MEFs were selected for further study (Figure 1A & Suppl. Fig. 1A).

We discovered that ritanserin strongly inhibited the proliferation of $Tsc2^{-/-}$ MEFs treated with CQ, while it had no effect on the viability of $Tsc2^{+/+}$ MEFs. Indeed, combination treatment with CQ (5uM) and ritanserin (10uM) inhibited the proliferation of $Tsc2^{-/-}$ MEFs by ~2.4-fold compared to untreated cells ($p<0.0001$; Figure 1A, B). Combination treatment with CQ and ritanserin strongly induced the apoptotic markers cleaved PARP and cleaved caspase 3 in $Tsc2^{-/-}$ MEFs (Fig. 1C). Interestingly, treatment of $Tsc2^{-/-}$ MEFs with a higher dose of ritanserin (20uM) selectively blocked the proliferation of $Tsc2^{-/-}$ MEFs as early as after 48 hours of treatment ($p<0.0001$; Figure 1D, E).

CQ inhibits autophagy by increasing the pH of acidic organelles including the lysosome. To determine whether the CQ effects were mediated by inhibition of the autophagic pathway we used $Tsc2^{+/+}$ and $Tsc2^{-/-}$ MEFs with Atg5 knockout (sgAtg5). As observed previously, ritanserin (20uM) selectively inhibited the proliferation of $Tsc2^{-/-}$ MEFs, independently of autophagy ($p<0.0001$; Figure 1F). These data suggest that the proliferation phenotype we observed in Tsc2-deficient cells following combination treatment with CQ and ritanserin most likely involves the lysosome.

Ritanserin has been recently identified as a potent inhibitor of Diacylglycerol Kinase Alpha (DGKA), a lipid kinase that produces the second messenger phosphatidic acid (PA). To determine whether the effects of ritanserin are due to phosphatidic acid depletion, we added phosphatidic acid (100uM) to $Tsc2^{-/-}$ MEFs treated with ritanserin (20uM). Phosphatidic acid add-back partially rescued the proliferation of $Tsc2^{-/-}$ MEFs (50% rescue, 72 hours, $p<0.0001$) suggesting that ritanserin inhibits the proliferation of Tsc2-deficient cells in part by depleting phosphatidic acid pools (Fig. 1G). Interestingly, add-back of PA (100uM) did not rescue the proliferation of EIPA-treated $Tsc2^{-/-}$ MEFs, further highlighting the specificity of the mechanism through which ritanserin depletes intracellular PA pools (Suppl. Fig. 1B).

To examine that growth suppression by ritanserin is caused by TSC2 loss, we examined the effects of this drug on two additional cell line models of TSC2 deficiency: MEFs derived from $Tsc2^{fl/fl}$ Rosa26-CreERT2 mice with tamoxifen-inducible loss of Tsc2 (Tsc2ko; Suppl. Fig. 1C, D), and TSC2-deficient human kidney-derived angiomyolipoma cells (Suppl. Fig.

1E, F). Combination treatment with CQ and ritanserin inhibited the proliferation of Tsc2ko MEFs (~2.5 fold; $p<0.0001$), while no difference was observed in Tsc2-expressing MEFs (Tsc2wt). In addition, treatment using 10uM and 20uM ritanserin inhibited the proliferation of TSC2-deficient angiolipoma (621–102 cells) by 20% and 50% respectively, compared to TSC2-expressing (621–103) cells ($p<0.0001$). We next wanted to determine whether ritanserin had any off-target effects in Tsc2-deficient cells. We treated Tsc2-deficient 105K mouse kidney cystadenoma cells with genetic inhibition of DGKA using increasing doses of ritanserin (Suppl. Fig. 1G). Interestingly, DGKA downregulation with two shRNA clones decreased the proliferation of 105K cells by 20% ($p<0.0001$) compared to shRNA control cells. Ritanserin treatment (1uM and 2uM; 72 hours) had no additional impact on the proliferation of shDGKA cells, indicating that the observed inhibition of proliferation is most likely not due to off-target drug effects. Higher doses of ritanserin (5uM and 10uM) inhibited the proliferation of shDGKA and shCtl cells equally. Additionally, the macropinocytosis inhibitor EIPA (6uM; 48 hours) selectively inhibited the proliferation of $Tsc2^{-/-}$ MEFs and not $Tsc2^{+/+}$ MEFs, suggesting that targeting macropinocytosis is a possible therapeutic approach in TSC and LAM (Suppl. Fig. 1H).

Genetic inhibition of DGKA synergizes with CQ to selectively inhibit the proliferation of TSC2-deficient cells

To determine the role of DGKA in the proliferation of Tsc2-deficient cells, we generated two cell lines with Tsc2-deficiency with stable *DGKA* downregulation. We used three shRNA clones to target DGKA in the Tsc2-deficient 105K and TTJ cells. Downregulation of *DGKA* gene and protein expression was confirmed by qRT-PCR and immunoblotting, respectively (Fig. 2A, B). Genetic inhibition of *DGKA* decreased the proliferation of 105K cells by 10–30% ($p<0.0001$, Fig. 2C–E). Interestingly, treatment with CQ (5uM) further inhibited the proliferation of 105K cells with *DGKA* downregulation by 70–90% ($p<0.0001$). Similarly, *DGKA* downregulation decreased proliferation of Tsc2-deficient TTJ cells by 20–45% ($p<0.0001$, Fig. 2F–H). As seen with 105K cells, *DGKA* downregulation sensitized TTJ cells to CQ treatment (5uM) and almost completely inhibited their growth (50–90%, $p<0.0001$). These data suggest that DGKA is required for Tsc2-deficient cell proliferation and creates a vulnerability to treatment with CQ. Moreover, our results on genetic inhibition of DGKA and CQ treatment confirm our earlier observations (Fig. 1) with combination treatment with CQ and ritanserin.

Since ritanserin treatment had a dramatic impact on the proliferation of TSC2-deficient cells, we focused on its role in TSC pathogenesis. First, we quantified the expression levels of DGKA in Tsc2-expressing and Tsc2-deficient cells. DGKA expression was increased by 2.7-fold in $Tsc2^{-/-}$ MEFs, compared to $Tsc2^{+/+}$ MEFs ($p<0.05$). Interestingly, rapamycin treatment (20nM; 24 hours) further increased expression of DGKA in $Tsc2^{-/-}$ MEFs by 5-fold ($p<0.001$), while Torin1 treatment (250nM; 24 hours) had no impact on DGKA expression (Fig. 2I). *DGKA* gene expression in $Tsc2^{+/+}$ MEFs was not affected by rapamycin or Torin1 treatments, indicating that increased *DGKA* expression in mTORC1-hyperactive cells may be a compensatory mechanism activated in response to mTORC1 inhibition. Secondly, *DGKA* expression was increased by 40% ($p<0.01$) in human angiomyolipomas (AML), compared to normal kidney tissues (Fig. 2J). There are nine

members in the diacylglycerol kinase family of proteins. We assessed the remaining DGKs and found that *DGKD*, *DGKQ* and *DGKZ* are also highly expressed in AML tissues compared to normal kidney tissue (Suppl. Fig. 2A). Finally, increased activity of DGKA has been associated with increased tumor progression in multiple cancers[33]. Therefore, we sought to determine the activity of DGKA in Tsc2-deficient cells. Indeed, DGKA activity was found to be increased in $Tsc2^{-/-}$ MEFs (2-fold; $p<0.01$) compared to $Tsc2^{+/+}$ MEFs (Fig. 2K). These results suggest that *DGKA* gene expression and activity are important in TSC and may play an important role in disease progression.

Ritanserin blocks macropinocytosis and lysosomal processing of nutrients in TSC2-deficient cells

We next hypothesized that ritanserin treatment inhibits the proliferation of TSC2-deficient cells, by reducing phosphatidic acid levels. In support of this hypothesis, we observed that add-back of PA, the metabolic product of DGKA, can rescue the proliferation of TSC2-deficient cells treated with ritanserin (Fig. 1G). To determine the role of ritanserin and DGKA in nutrient uptake via macropinocytosis we measured exogenous nutrient uptake using fluorescently labeled dextran (0.5mg/ml, 70kDa) and albumin (BSA-TMR; 0.5mg/ml). In support of previously published data[11], macropinocytosis is increased by three-fold in $Tsc2^{-/-}$ MEFs compared to $Tsc2^{+/+}$ MEFs (Fig. 3A). Additionally, treatment of $Tsc2^{-/-}$ MEFs with ritanserin (10uM; 16hrs) inhibited dextran uptake almost completely (90%, $p<0.0001$, Fig. 3A, C, Suppl. Fig. 3A). Adding back PA (100uM) to ritanserin treated $Tsc2^{-/-}$ MEFs restored macropinocytosis, indicating that ritanserin indeed inhibits macropinocytosis by depleting intracellular pools of PA. To further characterize the impact of ritanserin on macropinocytosis in the setting of TSC2 deficiency, we quantified the uptake of fluorescent albumin, (BSA, 0.5mg/ml). Treatment with ritanserin (10uM; 16 hours), inhibited the uptake of BSA by ~70% ($p<0.0001$; Fig. 3B, Suppl. Fig. 3B). As expected, treatment with the macropinocytosis inhibitor EIPA (25uM; 16hrs) also decreased dextran and BSA uptake by ~70% ($p<0.0001$). To ensure that cells being assessed for macropinocytosis are not undergoing cell death, we quantified cell proliferation following drug treatments. There was no observed impact on the proliferation of $Tsc2^{+/+}$ and $Tsc2^{-/-}$ MEFs at the 16-hour time point (Suppl. Fig. 3C). Interestingly, treatment with PA (100uM; 16hrs) increased the uptake of dextran (~15%) and BSA (~20%; Fig. 3A & 3B) and induced the phosphorylation of S6 kinase, downstream of mTORC1 in both $Tsc2^{+/+}$ and $Tsc2^{-/-}$ MEFs (Suppl. Fig. 3D). This finding suggests that PA induces mTORC1 activation downstream of TSC2 and further highlights the dependency of TSC2-deficient cells on DGKA-mediated macropinocytosis. To further confirm that macropinocytosis is mediated via DGKA, we performed the dextran uptake assays in TSC2-expressing (105K+TSC2) and TSC2-deficient (105K-EV) cells with stable downregulation of DGKA. Genetic inhibition of DGKA decreased macropinocytosis-mediated uptake of dextran in TSC2-deficient cells by ~45% ($p<0.0001$) and had minimal impact on the uptake of dextran in TSC2-expressing 105K cells (Fig. 3D). These data suggest that the enhanced macropinocytosis in TSC2-deficient cells is in part mediated by DGKA.

Macropinocytosis-mediated nutrient uptake and endocytic trafficking requires phosphatidic acid for successful delivery to the lysosome for degradation via the endolysosomal

network[24]. To assess the impact of ritanserin on the endolysosomal homeostasis of TSC2-deficient cells, we used lysotracker to quantify acidic organelles, including lysosomes, following ritanserin treatment. Interestingly, $Tsc2^{-/-}$ MEFs have an increased number of acidic organelles compared to $Tsc2^{+/+}$ MEFs as shown by lysotracker staining. Ritanserin treatment (10uM; 16hrs) decreased the number acidic organelles in $Tsc2^{-/-}$ MEFs by 45% ($p<0.0001$, Fig. 3E, Suppl. Fig. 3E). Combination treatment with CQ (5uM) and ritanserin further limited acidic organelles in $Tsc2^{-/-}$ MEFs (80%, $p<0.0001$). Inhibition of mTORC1 activity using rapamycin (20nM; 16 hours) strongly inhibited acidic organelles only in $Tsc2^{-/-}$ MEFs suggesting that mTORC1 activity is necessary for maintaining endolysosomal homeostasis. To determine whether this finding is limited to DGKA inhibition, we targeted macropinocytosis with EIPA (25uM; 16 hours), which also inhibited acidic organelles in $Tsc2^{-/-}$ MEFs (Suppl. Fig. 3F). To determine the impact of inhibiting macropinocytosis on the lysosomal function of $Tsc2^{-/-}$ MEFs, we employed a fluorogenic substrate (DQ-BSA) that emits fluorescence upon lysosomal proteolysis. We observed that lysosomal activity in $Tsc2^{-/-}$ MEFs was increased ~1.5-fold compared to $Tsc2^{+/+}$ MEFs ($p<0.0001$; Fig. 3F). Interestingly, ritanserin treatment inhibited lysosomal activity by 67% ($p<0.0001$; Fig. 3G). In summary, these findings indicate that DGKA plays a critical role in regulating macropinocytosis, lysosomal number and lysosomal activity. Furthermore, our results identify ritanserin as a potent macropinocytosis inhibitor in mTORC1-hyperactive cells that functions by depleting intracellular phosphatidic acid pools.

Ritanserin treatment induces metabolic reprogramming in TSC2-deficient cells

Since we observed a reduction in macropinocytosis and lysosomal function following ritanserin treatment, we investigated the role of ritanserin in the metabolism of TSC2-deficient cells by performing targeted metabolomics. $Tsc2^{-/-}$ MEFs treated with ritanserin (10uM; 16hrs) showed a distinct metabolic signature (Fig. 4A). Pathway enrichment analysis revealed the strong induction of metabolic pathways including phospholipid synthesis (Fig. 4B). Purine metabolism and phospholipid metabolism were among the most enriched metabolic pathways upon ritanserin treatment. Importantly, ritanserin treatment decreased most of the intermediate metabolites belonging to the pentose phosphate pathway (Fig. 4C–G). The pentose phosphate pathway (PPP), which is often upregulated in cancer, is the main source of cellular NADPH and ribose-5 phosphate for nucleotide synthesis. Indeed, the metabolic product of the PPP, ribose-5 phosphate (R-5P) was decreased by 35% following ritanserin treatment ($p<0.05$; Fig. 4G). The two purine nucleotides derived from R-5P, adenine and guanine, were also decreased by 30% ($p<0.01$) and 67% ($p<0.01$) respectively following ritanserin treatment, indicating that ritanserin induces nucleotide metabolic reprogramming in Tsc2-deficient cells (Fig. 4H–I). To determine whether ritanserin is involved in the modulation of the PPP, we assessed the expression of Glucose 5-phosphate dehydrogenase (G6PD) and Phosphogluconate dehydrogenase (PGD; Suppl. Fig. 4A, B). G6PD and PGD are part of the oxidative branch of the PPP and regulate the initial steps of PPP-derived nucleotides. Ritanserin increased the expression of PGD but not G6PD in $Tsc2^{-/-}$ MEFs, indicating that the observed metabolic reprogramming upon ritanserin treatment is caused due to depletion of nutrients upstream of the PPP. Furthermore, the nucleosides xanthosine and inosine where decreased following ritanserin treatment in $Tsc2^{-/-}$ MEFs. The pyrimidines cytosine, thymine and uracil were not impacted, suggesting

that ritanserin-induced metabolic alterations are specific to purine rather than pyrimidine synthesis (Suppl. Fig. 4C, 4D). Interestingly, decreased PPP activity and low NADPH levels lead to reduced lipid synthesis in diabetes and cancer[46]. Therefore, our findings indicate that ritanserin may impact lipid homeostasis by depleting DGKA-dependent PA pools (Fig. 3A, 3B) and by decreasing pentose phosphate pathway metabolites in TSC2-deficient cells.

Ritanserin rewires phospholipid metabolism in TSC2-deficient cells

Our targeted metabolomics analysis indicated that the phospholipid biosynthesis pathway was enriched upon ritanserin treatment ($p<0.001$; Fig. 4B). To further characterize the metabolic impact of ritanserin treatment in Tsc2-deficient cells, we used liquid chromatography-mass spectrometry to perform lipidomic analysis in $Tsc2^{-/-}$ MEFs treated with ritanserin (10uM; 16hrs) or vehicle control. Interestingly, phosphatidic acid (PA) levels were elevated 2.5-fold ($p<0.01$) in $Tsc2^{-/-}$ MEFs compared to $Tsc2^{+/+}$ MEFs (Fig. 5B & Suppl. Fig. 5A). Treatment with ritanserin resulted in a striking decrease of PA compared to vehicle treated $Tsc2^{-/-}$ MEFs (80%; $p<0.0001$). Interestingly, PA levels in $Tsc2^{+/+}$ MEFs were not impacted by ritanserin treatment. As expected, ritanserin increased diacylglycerol levels, the metabolic precursor of PA, by ~30% ($p<0.05$) and ~2 fold in $Tsc2^{-/-}$ MEFs and $Tsc2^{+/+}$ MEFs respectively (Fig. 5C & Suppl. Fig. 5B). Accumulation of diacylglycerol following ritanserin treatment led to subsequent increase in multiple phospholipids, including phosphatidylinositol (PI, 2-fold, $p<0.05$), lysophosphatidylcholine (LPC, 50%, $p<0.01$), phosphatidylserine (PS, 60%, $p<0.05$) and phosphatidylethanolamine (PE, 40%, $p<0.05$) in $Tsc2^{-/-}$ MEFs (Fig. 5D–G & Suppl. Fig. 5C–F). Similar changes were observed in ritanserin treated $Tsc2^{+/+}$ MEFs. These findings provide further evidence that ritanserin targets DGKA-mediated metabolism of diacylglycerol to phosphatidic acid specifically in Tsc2-deficient cells, creating a metabolic dependency.

Diacylglycerol and phosphatidic acid play a fundamental role in cellular metabolic homeostasis, functioning both as components of membranes as well as intermediates in lipid metabolism (Fig. 5A). Interestingly, diacylglycerol can be metabolized to produce triglycerides or phospholipids. Triglycerides and cholesterol are polar lipid moieties that are used for lipid storage in the form of lipid droplets[47]. To further characterize the impact of ritanserin on the lipidome of Tsc2-deficient cells, we visualized lipid droplets using confocal microscopy in Tsc2-expressing and Tsc2-deficient cells treated with ritanserin or vehicle control. Lipid droplet staining using BODIPY (10uM, BODIPY 493/503) revealed that ritanserin treatment reduces the formation of lipid droplets in $Tsc2^{-/-}$ MEFs by 50% ($p<0.05$) compared to untreated cells (Fig. 6A–B). Interestingly, ritanserin had no impact on lipid droplets in $Tsc2^{+/+}$ MEFs (Fig. 6C). These data suggest diacylglycerol accumulation following ritanserin treatment depletes storage of lipids in the form of lipid droplets, in favor of phospholipid biosynthesis.

Therapeutic targeting of DGKA suppresses tumorigenesis in preclinical models of TSC and LAM

We next sought to determine whether targeting DGKA can be a potential therapeutic approach for patients with TSC and LAM. We assessed the ability of Tsc2-deficient cells with genetic downregulation of DGKA to form lung lesions using a preclinical model of

LAM[44]. Indeed, DGKA downregulation prevented alveolar enlargement in the lungs of mice injected with Tsc2-deficient TTJ cells by 30% compared to Tsc2-deficient cells expressing control shRNA ($p<0.01$; Fig. 7A). Importantly, lungs with TSC2-deficient lesions contained multiple enlarged airspace regions, which were dispersed throughout the lung (Fig. 7B *upper panels*). In Tsc2-deficient lesions with DGKA downregulation, the alveolar airspace was decreased, suggesting that DGKA can be therapeutically targeted in LAM (Fig. 7B *lower panels*). Consistent with previous reports, mice injected with TTJ-shCtl cells progressively lost weight which is indicative of disease progression (Fig. 7C). In contrast, there was no change in body weight of mice injected with TTJ-shDGKA-3.

To assess the impact of ritanserin treatment on mTORC1-driven tumorigenesis, we used $Tsc2^{+/-}$ mice, which develop renal cysts and cystadenomas and better recapitulates human TSC[48]. Seven-month AJ $Tsc2^{+/-}$ mice (10 per group) were treated with ritanserin (20mg/kg/daily) or vehicle control for 30 days and the tumor burden was assessed. Interestingly, ritanserin treatment reduced the number of lesions per kidney by 33% ($p<0.0001$; Fig. 7D) as well as the overall kidney tumor volume by 25% ($p<0.05$; Fig. 7E, 7F). These data suggest that targeting DGKA may be a novel therapeutic approach for patients with TSC and LAM.

DISCUSSION

In this study, we performed a high-throughput drug screen to identify compounds that target the metabolic vulnerabilities of TSC2-deficient cells. We used chloroquine because previous studies have suggested that the low levels of autophagy (a consequence of mTORC1 hyperactivation) result in metabolic rewiring in TSC[36]. We discovered that ritanserin (10uM), in combination with CQ, selectively inhibits the proliferation of Tsc2-deficient MEFs (Fig. 1 & Suppl. Fig. 1). Surprisingly, when used at a higher dose (20uM), ritanserin completely blocks the proliferation of $Tsc2^{-/-}$ MEFs with minimal impact on $Tsc2^{+/+}$ MEFs. Although ritanserin was initially identified as a serotonin receptor antagonist, multiple subsequent studies have shown that it potently inhibits the lipid kinase DGKA[27,32]. We discovered that *DGKA* expression and activity are increased in $Tsc2^{-/-}$ MEFs (Fig. 2). This is particularly interesting, since recent work has shown that *DGKA, DGKD, DGKQ* and *DGKZ* are elevated in TSC patient-derived angiomyolipomas[40]. Since DGKA regulates cellular membrane homeostasis[24], and macropinocytosis is a critical survival mechanism of TSC2-deficient cells[11], we examined the impact of ritanserin on macropinocytic nutrient uptake.

We discovered that ritanserin is a potent macropinocytosis inhibitor in TSC2-deficient cells (Fig. 3). This discovery is interesting and important since, macropinocytosis is upregulated in many human tumors and is an especially important nutrient acquisition mechanism in pancreatic cancer[13,18,49]. In addition, aberrant activation of mTORC1 is associated with most human malignancies[50]. To date, it has been challenging to target macropinocytosis, since the most widely used inhibitor EIPA (amiloride) is an antihypertensive[51]. Ritanserin, which has a very favorable safety profile, could be useful both experimentally and in clinical trials.

An increasing body of evidence indicates that phospholipids play a critical role in macropinocytosis[52]. In cancer cells, macropinocytosis is in part driven by activation of phospholipid synthesis enzymes including, phosphoinositide 3-kinase (PI3K), and phospholipase C (PLC)[53–55]. Diacylglycerol kinases are also known to be recruited to the plasma membrane where they initiate membrane ruffling (the first step in macropinocytosis) via activation of protein kinase c (PKC) and Rac1[56]. Interestingly, our lipidomic analysis revealed that ritanserin inhibits DGKA-mediated metabolism of diacylglycerol, which results in depletion of phosphatidic acid and inhibition of macropinocytosis in TSC2-deficient cells (Figs. 3 & 5). Lipid metabolism is altered in TSC and LAM, especially since LAM cells and serum from LAM patients exhibit a distinct lipidomic signature with elevated Lysophosphatidylcholine (LPC), fatty acids and phospholipids compared to healthy women[57–59]. Additionally, renal angiomyolipomas (AMLs), the most prevalent tumor in TSC and LAM patients, are characterized by increased lipid accumulation as a consequence of aberrant mTORC1 activation[60,61]. We discovered that ritanserin rewires the phospholipid metabolism of TSC2-deficient cells by depleting neutral lipid storage (lipid droplets) while enhancing synthesis of more bioenergetically favorable phospholipids (Fig. 6). These data taken together with our lipidomic analyses indicate that DGKA plays a crucial role maintaining phospholipid homeostasis and uncover a novel link between macropinocytosis and lipid metabolism in TSC2-deficient cells.

Identifying ritanserin as a potential treatment for TSC is particularly interesting, since earlier drug screens performed in TSC2-deficient cells have also identified SSRIs and antipsychotics as possible therapeutic approaches[62,63]. In addition, ritanserin has demonstrated efficacy in mouse models of metastatic brain tumors[64] and in lung cancer[32]. Ritanserin has been used in several clinical trials and exhibits a promising pharmacologic profile, including an extensive half-life window (40 hours) and blood-brain barrier penetration[65]. Therefore, this agent could be rapidly translated to clinical practice, with potential impact for patients with TSC and LAM, as well as for macropinocytic tumors such as pancreatic cancer.

Supplementary Material

Refer to Web version on PubMed Central for supplementary material.

Acknowledgments:

The LAM Foundation Career Development Award, Wade Family TSC Research Fund, Tuberous Sclerosis Alliance Preclinical Consortium, NIH-NIDDK: 5R01DK102146-05. The graphical abstract was created with BioRender.com

REFERENCES

1. Henske EP, Jozwiak S, Kingswood JC, Sampson JR & Thiele EA Tuberous sclerosis complex. Nat Rev Dis Primers 2, 16035, doi:10.1038/nrdp.2016.35 (2016). [PubMed: 27226234]
2. Johnson SR, Taveira-DaSilva AM & Moss J Lymphangioleiomyomatosis. Clin Chest Med 37, 389–403, doi:10.1016/j.ccm.2016.04.002 (2016). [PubMed: 27514586]
3. Meraj R, Wikenheiser-Brokamp KA, Young LR & McCormack FX Lymphangioleiomyomatosis: new concepts in pathogenesis, diagnosis, and treatment. Semin Respir Crit Care Med 33, 486–497, doi:10.1055/s-0032-1325159 (2012). [PubMed: 23001803]

4. Taveira-DaSilva AM & Moss J Clinical features, epidemiology, and therapy of lymphangioleiomyomatosis. Clin Epidemiol 7, 249–257, doi:10.2147/CLEP.S50780 (2015). [PubMed: 25897262]
5. McCormack FX, Inoue Y, Moss J, Singer LG, Strange C, Nakata K et al. Efficacy and safety of sirolimus in lymphangioleiomyomatosis. N Engl J Med 364, 1595–1606, doi:10.1056/NEJMoa1100391 (2011). [PubMed: 21410393]
6. Carsillo T, Astrinidis A & Henske EP Mutations in the tuberous sclerosis complex gene TSC2 are a cause of sporadic pulmonary lymphangioleiomyomatosis. Proc Natl Acad Sci U S A 97, 6085–6090, doi:10.1073/pnas.97.11.6085 (2000). [PubMed: 10823953]
7. Yu J, Astrinidis A & Henske EP Chromosome 16 loss of heterozygosity in tuberous sclerosis and sporadic lymphangiomyomatosis. Am J Respir Crit Care Med 164, 1537–1540, doi:10.1164/ajrccm.164.8.2104095 (2001). [PubMed: 11704609]
8. Ben-Sahra I & Manning BD mTORC1 signaling and the metabolic control of cell growth. Curr Opin Cell Biol 45, 72–82, doi:10.1016/j.ceb.2017.02.012 (2017). [PubMed: 28411448]
9. Holz MK, Ballif BA, Gygi SP & Blenis J mTOR and S6K1 mediate assembly of the translation preinitiation complex through dynamic protein interchange and ordered phosphorylation events. Cell 123, 569–580, doi:10.1016/j.cell.2005.10.024 (2005). [PubMed: 16286006]
10. Choo AY, Kim SG, Vander Heiden MG, Mahoney SJ, Vu H, Yoon SO et al. Glucose addiction of TSC null cells is caused by failed mTORC1-dependent balancing of metabolic demand with supply. Mol Cell 38, 487–499, doi:10.1016/j.molcel.2010.05.007 (2010). [PubMed: 20513425]
11. Filippakis H, Belaid A, Siroky B, Wu C, Alesi N, Hougard T et al. Vps34-mediated macropinocytosis in Tuberous Sclerosis Complex 2-deficient cells supports tumorigenesis. Sci Rep 8, 14161, doi:10.1038/s41598-018-32256-x (2018). [PubMed: 30242175]
12. Filippakis H, Alesi N, Ogorek B, Nijmeh J, Khabibullin D, Gutierrez C et al. Lysosomal regulation of cholesterol homeostasis in tuberous sclerosis complex is mediated via NPC1 and LDL-R. Oncotarget 8, 38099–38112, doi:10.18632/oncotarget.17485 (2017). [PubMed: 28498820]
13. Commisso C, Davidson SM, Soydaner-Azeloglu RG, Parker SJ, Kamphorst JJ, Hackett S et al. Macropinocytosis of protein is an amino acid supply route in Ras-transformed cells. Nature 497, 633–637, doi:10.1038/nature12138 (2013). [PubMed: 23665962]
14. Palm W, Park Y, Wright K, Pavlova NN, Tuveson DA & Thompson CB The Utilization of Extracellular Proteins as Nutrients Is Suppressed by mTORC1. Cell 162, 259–270, doi:10.1016/j.cell.2015.06.017 (2015). [PubMed: 26144316]
15. Swanson JA Shaping cups into phagosomes and macropinosomes. Nat Rev Mol Cell Biol 9, 639–649, doi:10.1038/nrm2447 (2008). [PubMed: 18612320]
16. Davidson SM & Vander Heiden MG Critical Functions of the Lysosome in Cancer Biology. Annu Rev Pharmacol Toxicol 57, 481–507, doi:10.1146/annurev-pharmtox-010715-103101 (2017). [PubMed: 27732799]
17. Recouvreux MV & Commisso C Macropinocytosis: A Metabolic Adaptation to Nutrient Stress in Cancer. Front Endocrinol (Lausanne) 8, 261, doi:10.3389/fendo.2017.00261 (2017). [PubMed: 29085336]
18. Kamphorst JJ, Nofal M, Commisso C, Hackett SR, Lu W, Grabocka E et al. Human pancreatic cancer tumors are nutrient poor and tumor cells actively scavenge extracellular protein. Cancer Res 75, 544–553, doi:10.1158/0008-5472.CAN-14-2211 (2015). [PubMed: 25644265]
19. Demetriades C, Doumpas N & Teleman AA Regulation of TORC1 in response to amino acid starvation via lysosomal recruitment of TSC2. Cell 156, 786–799, doi:10.1016/j.cell.2014.01.024 (2014). [PubMed: 24529380]
20. Fang Y, Vilella-Bach M, Bachmann R, Flanigan A & Chen J Phosphatidic acid-mediated mitogenic activation of mTOR signaling. Science 294, 1942–1945, doi:10.1126/science.1066015 (2001). [PubMed: 11729323]
21. Toschi A, Lee E, Xu L, Garcia A, Gadir N & Foster DA Regulation of mTORC1 and mTORC2 complex assembly by phosphatidic acid: competition with rapamycin. Mol Cell Biol 29, 1411–1420, doi:10.1128/MCB.00782-08 (2009). [PubMed: 19114562]

22. Bohdanowicz M & Grinstein S Role of phospholipids in endocytosis, phagocytosis, and macropinocytosis. Physiol Rev 93, 69–106, doi:10.1152/physrev.00002.2012 (2013). [PubMed: 23303906]
23. Swanson JA Phorbol esters stimulate macropinocytosis and solute flow through macrophages. J Cell Sci 94 (Pt 1), 135–142 (1989). [PubMed: 2613767]
24. Bohdanowicz M, Schlam D, Hermansson M, Rizzuti D, Fairn GD, Ueyama T et al. Phosphatidic acid is required for the constitutive ruffling and macropinocytosis of phagocytes. Mol Biol Cell 24, 1700–1712, S1701–1707, doi:10.1091/mbc.E12-11-0789 (2013). [PubMed: 23576545]
25. Luo B, Regier DS, Prescott SM & Topham MK Diacylglycerol kinases. Cell Signal 16, 983–989, doi:10.1016/j.cellsig.2004.03.016 (2004). [PubMed: 15212759]
26. Sakane F, Imai S, Kai M, Yasuda S & Kanoh H Diacylglycerol kinases as emerging potential drug targets for a variety of diseases. Curr Drug Targets 9, 626–640, doi:10.2174/138945008785132394 (2008). [PubMed: 18691010]
27. Boroda S, Niccum M, Raje V, Purow BW & Harris TE Dual activities of ritanserin and R59022 as DGKalpha inhibitors and serotonin receptor antagonists. Biochem Pharmacol 123, 29–39, doi:10.1016/j.bcp.2016.10.011 (2017). [PubMed: 27974147]
28. Franks CE, Campbell ST, Purow BW, Harris TE & Hsu KL The Ligand Binding Landscape of Diacylglycerol Kinases. Cell Chem Biol 24, 870–880 e875, doi:10.1016/j.chembiol.2017.06.007 (2017). [PubMed: 28712745]
29. Wiesel FA, Nordstrom AL, Farde L & Eriksson B An open clinical and biochemical study of ritanserin in acute patients with schizophrenia. Psychopharmacology (Berl) 114, 31–38, doi:10.1007/BF02245441 (1994). [PubMed: 7846205]
30. Cornish JW, Maany I, Fudala PJ, Ehrman RN, Robbins SJ & O'Brien CP A randomized, double-blind, placebo-controlled study of ritanserin pharmacotherapy for cocaine dependence. Drug Alcohol Depend 61, 183–189, doi:10.1016/s0376-8716(00)00140-x (2001). [PubMed: 11137283]
31. Leysen JE, Gommeren W, Van Gompel P, Wynants J, Janssen PF & Laduron PM Receptor-binding properties in vitro and in vivo of ritanserin: A very potent and long acting serotonin-S2 antagonist. Mol Pharmacol 27, 600–611 (1985). [PubMed: 2860558]
32. Campbell ST, Franks CE, Borne AL, Shin M, Zhang L & Hsu KL Chemoproteomic Discovery of a Ritanserin-Targeted Kinase Network Mediating Apoptotic Cell Death of Lung Tumor Cells. Mol Pharmacol 94, 1246–1255, doi:10.1124/mol.118.113001 (2018). [PubMed: 30158316]
33. Olmez I, Love S, Xiao A, Manigat L, Randolph P, McKenna BD et al. Targeting the mesenchymal subtype in glioblastoma and other cancers via inhibition of diacylglycerol kinase alpha. Neuro Oncol 20, 192–202, doi:10.1093/neuonc/nox119 (2018). [PubMed: 29048560]
34. Zhang H, Cicchetti G, Onda H, Koon HB, Asrican K, Bajraszewski N et al. Loss of Tsc1/Tsc2 activates mTOR and disrupts PI3K-Akt signaling through downregulation of PDGFR. J Clin Invest 112, 1223–1233, doi:10.1172/JCI17222 (2003). [PubMed: 14561707]
35. Ogorek B, Lam HC, Khabibullin D, Liu HJ, Nijmeh J, Triboulet R et al. TSC2 regulates microRNA biogenesis via mTORC1 and GSK3beta. Hum Mol Genet 27, 1654–1663, doi:10.1093/hmg/ddy073 (2018). [PubMed: 29509898]
36. Parkhitko AA, Priolo C, Coloff JL, Yun J, Wu JJ, Mizumura K et al. Autophagy-dependent metabolic reprogramming sensitizes TSC2-deficient cells to the antimetabolite 6-aminonicotinamide. Mol Cancer Res 12, 48–57, doi:10.1158/1541-7786.MCR-13-0258-T (2014). [PubMed: 24296756]
37. Maisel K, Merrilees MJ, Atochina-Vasserman EN, Lian L, Obraztsova K, Rue R et al. Immune Checkpoint Ligand PD-L1 Is Upregulated in Pulmonary Lymphangioleiomyomatosis. Am J Respir Cell Mol Biol 59, 723–732, doi:10.1165/rcmb.2018-0123OC (2018). [PubMed: 30095976]
38. Siroky BJ, Yin H, Babcock JT, Lu L, Hellmann AR, Dixon BP et al. Human TSC-associated renal angiomyolipoma cells are hypersensitive to ER stress. Am J Physiol Renal Physiol 303, F831–844, doi:10.1152/ajprenal.00441.2011 (2012). [PubMed: 22791333]
39. Corsello SM, Bittker JA, Liu Z, Gould J, McCarren P, Hirschman JE et al. The Drug Repurposing Hub: a next-generation drug library and information resource. Nat Med 23, 405–408, doi:10.1038/nm.4306 (2017). [PubMed: 28388612]

40. Martin KR, Zhou W, Bowman MJ, Shih J, Au KS, Dittenhafer-Reed KE et al. The genomic landscape of tuberous sclerosis complex. Nat Commun 8, 15816, doi:10.1038/ncomms15816 (2017). [PubMed: 28643795]
41. Dobin A, Davis CA, Schlesinger F, Drenkow J, Zaleski C, Jha S et al. STAR: ultrafast universal RNA-seq aligner. Bioinformatics 29, 15–21, doi:10.1093/bioinformatics/bts635 (2013). [PubMed: 23104886]
42. Weigel C, Veldwijk MR, Oakes CC, Seibold P, Slynko A, Liesenfeld DB et al. Epigenetic regulation of diacylglycerol kinase alpha promotes radiation-induced fibrosis. Nat Commun 7, 10893, doi:10.1038/ncomms10893 (2016). [PubMed: 26964756]
43. Breitkopf SB, Ricoult SJH, Yuan M, Xu Y, Peake DA, Manning BD et al. A relative quantitative positive/negative ion switching method for untargeted lipidomics via high resolution LC-MS/MS from any biological source. Metabolomics 13, doi:10.1007/s11306-016-1157-8 (2017).
44. Goncharova EA, Goncharov DA, Fehrenbach M, Khavin I, Ducka B, Hino O et al. Prevention of alveolar destruction and airspace enlargement in a mouse model of pulmonary lymphangioleiomyomatosis (LAM). Sci Transl Med 4, 154ra134, doi:10.1126/scitranslmed.3003840 (2012).
45. Lee L, Sudentas P, Donohue B, Asrican K, Worku A, Walker V et al. Efficacy of a rapamycin analog (CCI-779) and IFN-gamma in tuberous sclerosis mouse models. Genes Chromosomes Cancer 42, 213–227, doi:10.1002/gcc.20118 (2005). [PubMed: 15578690]
46. Ge T, Yang J, Zhou S, Wang Y, Li Y & Tong X The Role of the Pentose Phosphate Pathway in Diabetes and Cancer. Front Endocrinol (Lausanne) 11, 365, doi:10.3389/fendo.2020.00365 (2020). [PubMed: 32582032]
47. Olzmann JA & Carvalho P Dynamics and functions of lipid droplets. Nat Rev Mol Cell Biol 20, 137–155, doi:10.1038/s41580-018-0085-z (2019). [PubMed: 30523332]
48. Kobayashi T, Minowa O, Kuno J, Mitani H, Hino O & Noda T Renal carcinogenesis, hepatic hemangiomatosis, and embryonic lethality caused by a germ-line Tsc2 mutation in mice. Cancer Res 59, 1206–1211 (1999). [PubMed: 10096549]
49. Kim SM, Roy SG, Chen B, Nguyen TM, McMonigle RJ, McCracken AN et al. Targeting cancer metabolism by simultaneously disrupting parallel nutrient access pathways. J Clin Invest 126, 4088–4102, doi:10.1172/JCI87148 (2016). [PubMed: 27669461]
50. Kelsey I & Manning BD mTORC1 status dictates tumor response to targeted therapeutics. Sci Signal 6, pe31, doi:10.1126/scisignal.2004632 (2013). [PubMed: 24065143]
51. Wei FF, Zhang ZY, Huang QF & Staessen JA Diagnosis and management of resistant hypertension: state of the art. Nat Rev Nephrol 14, 428–441, doi:10.1038/s41581-018-0006-6 (2018). [PubMed: 29700488]
52. Levin R, Grinstein S & Schlam D Phosphoinositides in phagocytosis and macropinocytosis. Biochim Biophys Acta 1851, 805–823, doi:10.1016/j.bbalip.2014.09.005 (2015). [PubMed: 25238964]
53. Amyere M, Payrastre B, Krause U, Van Der Smissen P, Veithen A & Courtoy PJ Constitutive macropinocytosis in oncogene-transformed fibroblasts depends on sequential permanent activation of phosphoinositide 3-kinase and phospholipase C. Mol Biol Cell 11, 3453–3467, doi:10.1091/mbc.11.10.3453 (2000). [PubMed: 11029048]
54. Araki N, Johnson MT & Swanson JA A role for phosphoinositide 3-kinase in the completion of macropinocytosis and phagocytosis by macrophages. J Cell Biol 135, 1249–1260, doi:10.1083/jcb.135.5.1249 (1996). [PubMed: 8947549]
55. Palm W, Araki J, King B, DeMatteo RG & Thompson CB Critical role for PI3-kinase in regulating the use of proteins as an amino acid source. Proc Natl Acad Sci U S A 114, E8628–E8636, doi:10.1073/pnas.1712726114 (2017). [PubMed: 28973876]
56. Chianale F, Rainero E, Cianflone C, Bettio V, Pighini A, Porporato PE et al. Diacylglycerol kinase alpha mediates HGF-induced Rac activation and membrane ruffling by regulating atypical PKC and RhoGDI. Proc Natl Acad Sci U S A 107, 4182–4187, doi:10.1073/pnas.0908326107 (2010). [PubMed: 20160093]

57. Priolo C, Ricoult SJ, Khabibullin D, Filippakis H, Yu J, Manning BD et al. Tuberous sclerosis complex 2 loss increases lysophosphatidylcholine synthesis in lymphangioleiomyomatosis. Am J Respir Cell Mol Biol 53, 33–41, doi:10.1165/rcmb.2014-0379RC (2015). [PubMed: 25780943]
58. Li C, Zhang E, Sun Y, Lee PS, Zhan Y, Guo Y et al. Rapamycin-insensitive up-regulation of adipocyte phospholipase A2 in tuberous sclerosis and lymphangioleiomyomatosis. PLoS One 9, e104809, doi:10.1371/journal.pone.0104809 (2014). [PubMed: 25347447]
59. Bottolo L, Miller S & Johnson SR Sphingolipid, fatty acid and phospholipid metabolites are associated with disease severity and mTOR inhibition in lymphangioleiomyomatosis. Thorax, doi:10.1136/thoraxjnl-2019-214241 (2020).
60. Crino PB, Nathanson KL & Henske EP The tuberous sclerosis complex. N Engl J Med 355, 1345–1356, doi:10.1056/NEJMra055323 (2006). [PubMed: 17005952]
61. Zhang HH, Huang J, Duvel K, Boback B, Wu S, Squillace RM et al. Insulin stimulates adipogenesis through the Akt-TSC2-mTORC1 pathway. PLoS One 4, e6189, doi:10.1371/journal.pone.0006189 (2009). [PubMed: 19593385]
62. Li J, Shin S, Sun Y, Yoon SO, Li C, Zhang E et al. mTORC1-Driven Tumor Cells Are Highly Sensitive to Therapeutic Targeting by Antagonists of Oxidative Stress. Cancer Res 76, 4816–4827, doi:10.1158/0008-5472.CAN-15-2629 (2016). [PubMed: 27197195]
63. Medvetz D, Sun Y, Li C, Khabibullin D, Balan M, Parkhitko A et al. High-throughput drug screen identifies chelerythrine as a selective inducer of death in a TSC2-null setting. Mol Cancer Res 13, 50–62, doi:10.1158/1541-7786.MCR-14-0440 (2015). [PubMed: 25185584]
64. Purow B Molecular Pathways: Targeting Diacylglycerol Kinase Alpha in Cancer. Clin Cancer Res 21, 5008–5012, doi:10.1158/1078-0432.CCR-15-0413 (2015). [PubMed: 26420856]
65. Akhondzadeh S, Malek-Hosseini M, Ghoreishi A, Raznahan M & Rezazadeh SA Effect of ritanserin, a 5HT2A/2C antagonist, on negative symptoms of schizophrenia: a double-blind randomized placebo-controlled study. Prog Neuropsychopharmacol Biol Psychiatry 32, 1879–1883, doi:10.1016/j.pnpbp.2008.08.020 (2008). [PubMed: 18801405]

Significance:

This study identifies macropinocytosis and phospholipid metabolism as novel mechanisms of metabolic homeostasis in mTORC1-hyperactive cells and suggest ritanserin as a novel therapeutic strategy for use in mTORC1-hyperactive tumors, including pancreatic cancer.

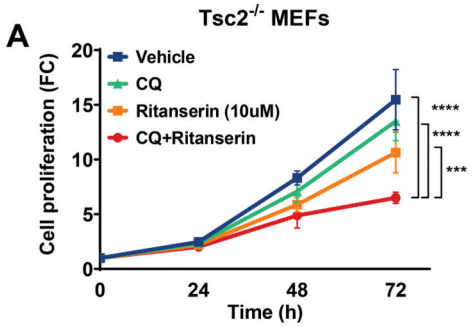

	Tsc2+/+		Tsc2-/-		
	Vehicle	CQ	Vehicle	CQ	
Compound	Relative viability (FC)				Drug Class
Ritanserin	1.0	0.8	0.8	-10.8	SSRI
Duloxetine	1.0	1.6	1.2	-8.4	SSRI
Chlorpromazine	1.0	0.1	0.8	-4.4	Dopamine rec. inh.
Chlorcyclizine	1.0	8.8	4.0	-3.6	Histamine H1 ant.
Blonanserin	1.0	0.8	1.2	-3.3	Dopamine rec. ant.
Eticlopride	1.0	0.4	0.5	-2.3	Dopamine rec. ant.
Fluvoxamine	1.0	0.9	0.2	-1.9	SSRI
Amorolfine	1.0	0.6	0.5	-1.8	Δ-14-reductase inh.
BD1047	1.0	1.3	0.5	-1.7	σ1 rec. ant.
Ro 60-0175	1.0	0.8	0.4	-1.4	5-HT2 rec. agonist

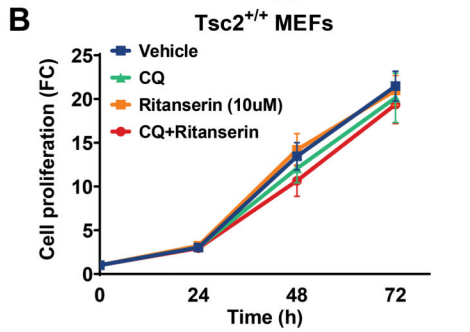

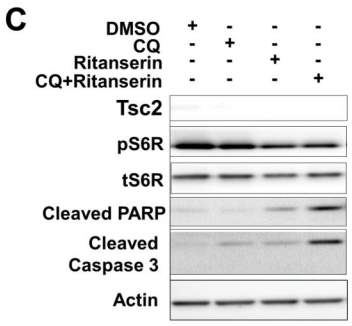

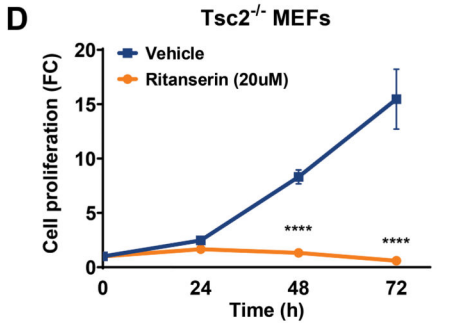

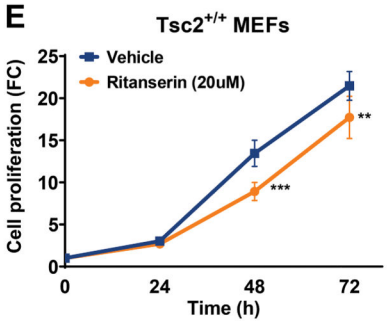

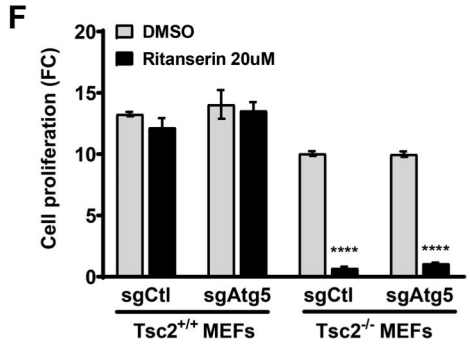

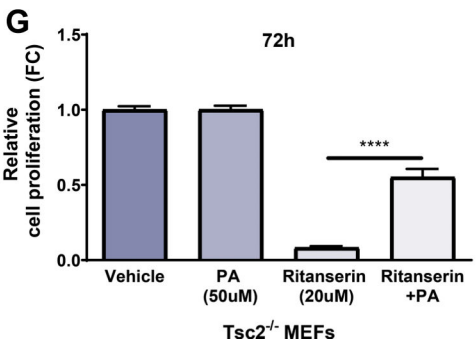

Figure 1. Chloroquine synergizes with ritanserin to selectively inhibit the proliferation of Tsc2-deficient cells.

(A) Combination treatment with CQ (5uM) and ritanserin (10uM) inhibits the proliferation of $Tsc2^{-/-}$ MEFs (left panel). Top ten compounds identified from the high-throughput drug screen (right panel). Ritanserin selectively decreased the proliferation of $Tsc2^{-/-}$ MEFs (~10-fold; compared to untreated $Tsc2^{+/+}$ MEFs). **(B)** Ritanserin or combination treatments had no impact on $Tsc2^{+/+}$ MEFs. **(C)** Immunoblotting shows that combination treatment with CQ (5uM) and ritanserin (10uM) induces apoptosis in $Tsc2^{-/-}$ MEFs (24 hours). **(D-E)**

Ritanserin (20uM) blocks the proliferation of $Tsc2^{-/-}$ MEFs but not $Tsc2^{+/+}$ MEFs. **(F)** Ritanserin inhibits the proliferation of $Tsc2^{-/-}$ MEFs regardless of their autophagic status. Values are shown as fold-change (FC) normalized to the day of seeding. **(G)** Ritanserin-mediated inhibition of proliferation is reversed by adding-back phosphatidic acid (100uM; 72 hours). Proliferation was quantified using crystal violet staining. Data represented as mean +/− standard deviation of six biological replicates. Statistical significance was assessed using two-way and one-way ANOVAs with Bonferroni correction with **p < 0.01, ***p < 0.001, ****p < 0.0001.

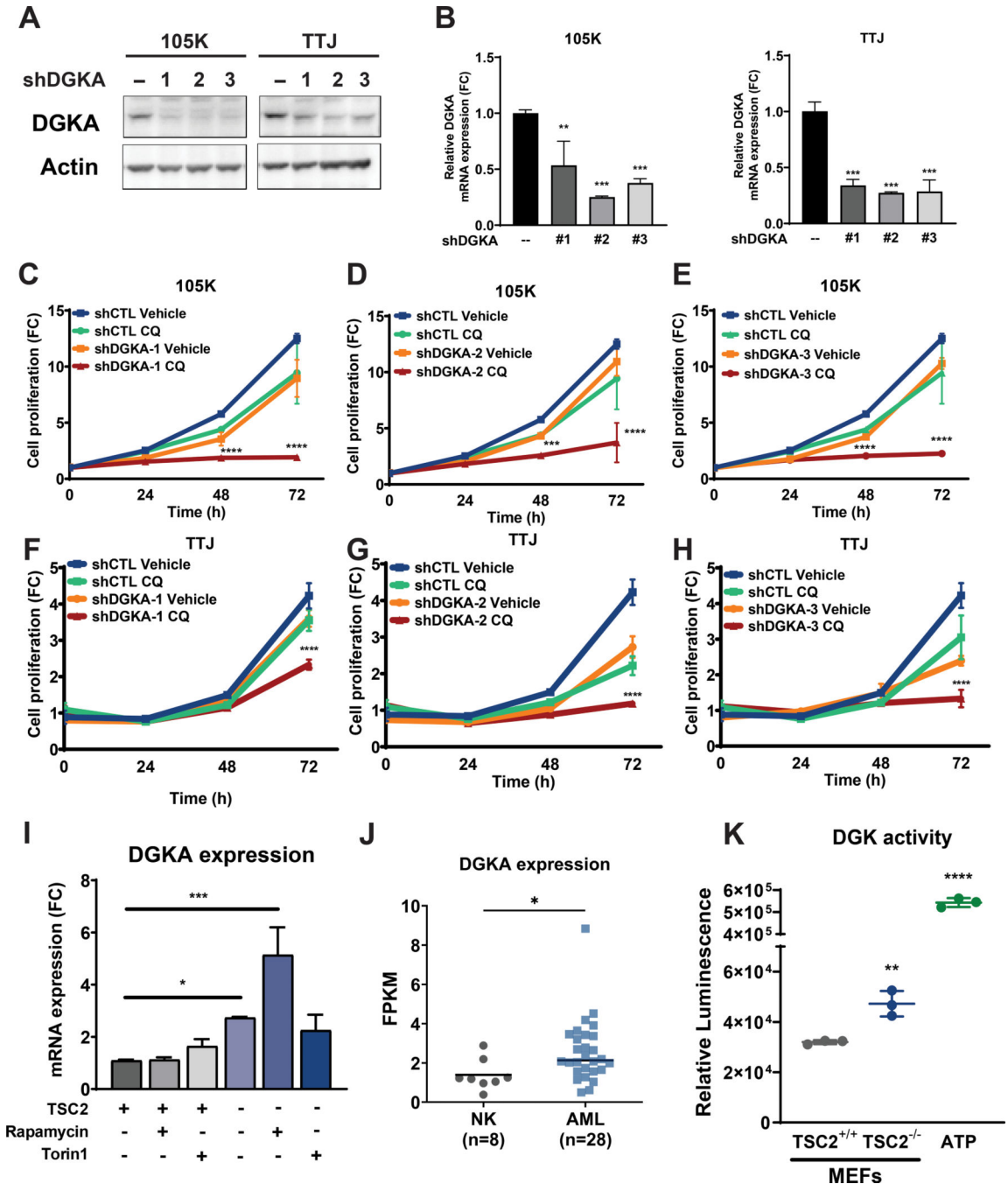

Figure 2. Genetic inhibition of DGKA sensitizes TSC2-deficient cells to chloroquine treatment.

(A) Immunoblots confirmed downregulation of *DGKA* in Tsc2-deficient 105K and TTJ cells. **(B)** Quantitative real-time PCR confirmed *DGKA* gene knockdown. **(C-E)** Genetic inhibition of DGKA sensitized Tsc2-deficient 105K cells to CQ (5uM). Three shRNA clones against DGKA were tested. **(F-H)** Genetic inhibition of DGKA sensitized Tsc2-deficient TTJ cells to CQ treatment (5uM). Proliferation was quantified using crystal violet staining. Values are shown as fold-change (FC) normalized to the day of seeding. **(I)** Quantitative real-time PCR shows increased expression of *Dgka* in $Tsc2^{-/-}$ MEFs compared to $Tsc2^{+/+}$

MEFs. Rapamycin treatment (20nM) further increased *Dgka* expression, while Torin1 (250nM) had no effect. Rapamycin and Torin1 had no impact on the expression of *Dgka* in $Tsc2^{+/+}$ MEFs. Data are from three biological replicates for each condition. **(J)** *Dgka* gene expression is elevated in renal angiomyolipoma tissues (n=28) compared to normal kidney tissues (n=8). Statistical significance was assessed using Mann-Whitney test (p=0.0191). **(K)** Diacylglycerol kinase activity is enhanced in $Tsc2^{-/-}$ MEFs compared to $Tsc2^{+/+}$ MEFs. ATP was used as a positive control. Data are represented as mean +/− standard deviation. For two-group comparisons, unpaired t-test was used. Two-way ANOVA test with Bonferroni correction was applied for comparing multiple groups. Statistical significance was determined as *p<0.05, **p<0.01, ***p<0.001, ****p < 0.0001.

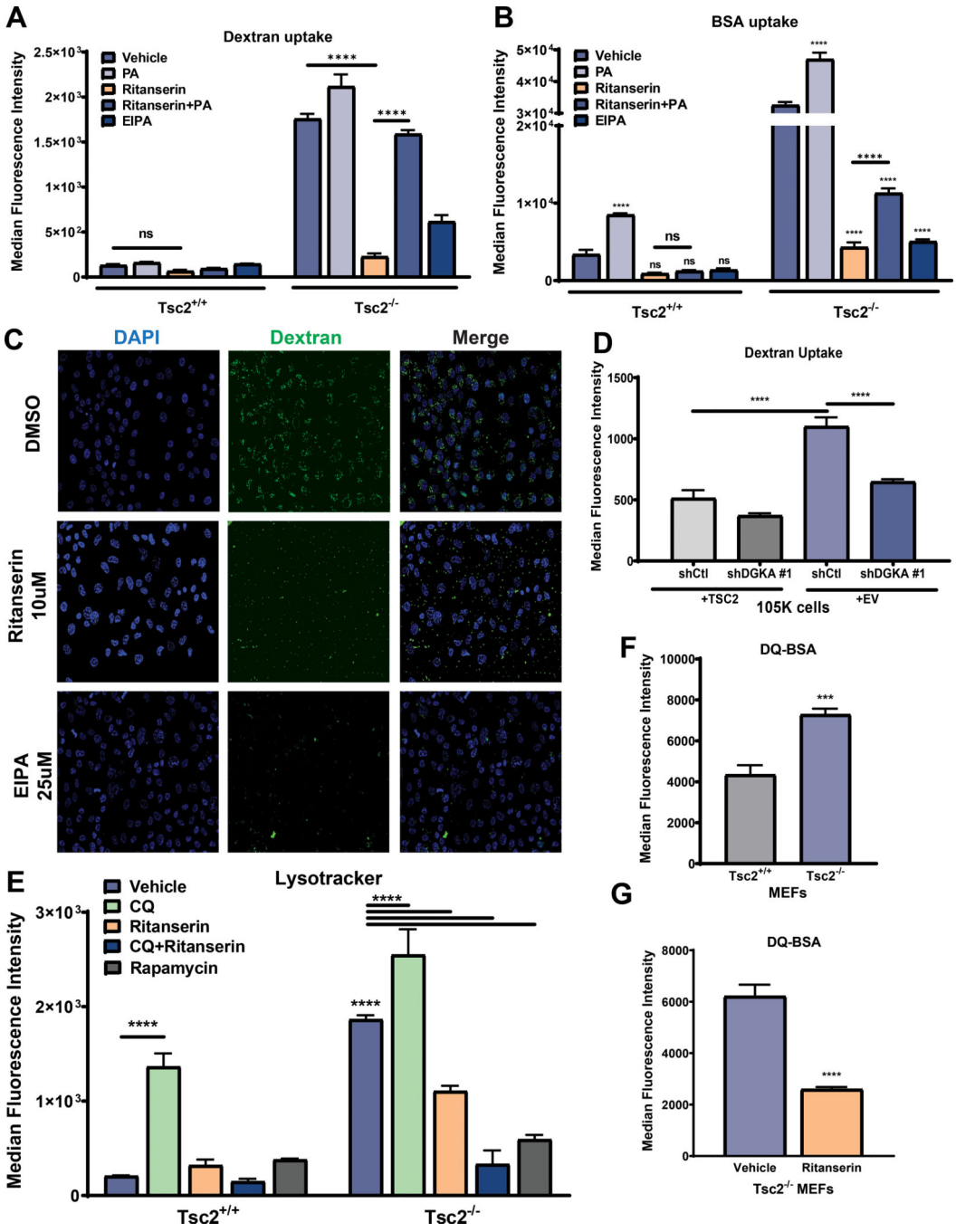

Figure 3. Enhanced macropinocytosis in Tsc2-deficient cells is mediated via DGKA.

(A) Macropinocytosis is enhanced (3-fold) in $Tsc2^{-/-}$ MEFs compared to $Tsc2^{+/+}$ MEFs. Ritanserin (10uM; 16 hours) inhibited the macropinocytic uptake of dextran (0.5mg/ml, FITC-Dextran) selectively in $Tsc2^{-/-}$ MEFs. PA (100uM) restored macropinocytosis of ritanserin-treated $Tsc2^{-/-}$ MEFs to levels compared to that of untreated cells. **(B)** Exogenous protein uptake (0.5mg/ml, BSA-TMR) was increased in ritanserin (10uM; 16 hours) treated $Tsc2^{-/-}$ MEFs compared to $Tsc2^{+/+}$ MEFs. PA (100uM) partially rescued macropinocytosis in $Tsc2^{-/-}$ MEFs. As expected, EIPA (25uM;16 hours) inhibited macropinocytic dextran and

BSA uptake. **(C)** Confocal microscopy shows that ritanserin inhibits macropinocytic uptake of dextran (10uM; 16 hours). **(D)** Genetic downregulation of DGKA inhibits macropinocytic dextran uptake (0.5mg/ml, FITC-Dextran). **(E)** Lysotracker staining revealed that ritanserin (10uM; 16 hours) reduces lysosome numbers in $Tsc2^{-/-}$ MEFs but not in $Tsc2^{+/+}$ MEFs. Combination treatment with CQ and ritanserin further inhibited lysosomal numbers. mTORC1 inhibitor rapamycin (20nM; 16 hours) strongly decreased lysosomes in $Tsc2^{-/-}$ MEFs but not in $Tsc2^{+/+}$ MEFs. **(F-G)** Lysosomal activity is enhanced in $Tsc2^{-/-}$ MEFs compared to $Tsc2^{+/+}$ MEFs. Ritanserin treatment (10uM; 16 hours) decreased lysosomal activity by 50% (0.2mg/ml; DQ-BSA). Data represented as mean +/− standard deviation from three biological replicates. Statistical significance was assessed using two-way ANOVA with Bonferroni correction with ***$p<0.001$, ****$p < 0.0001$.

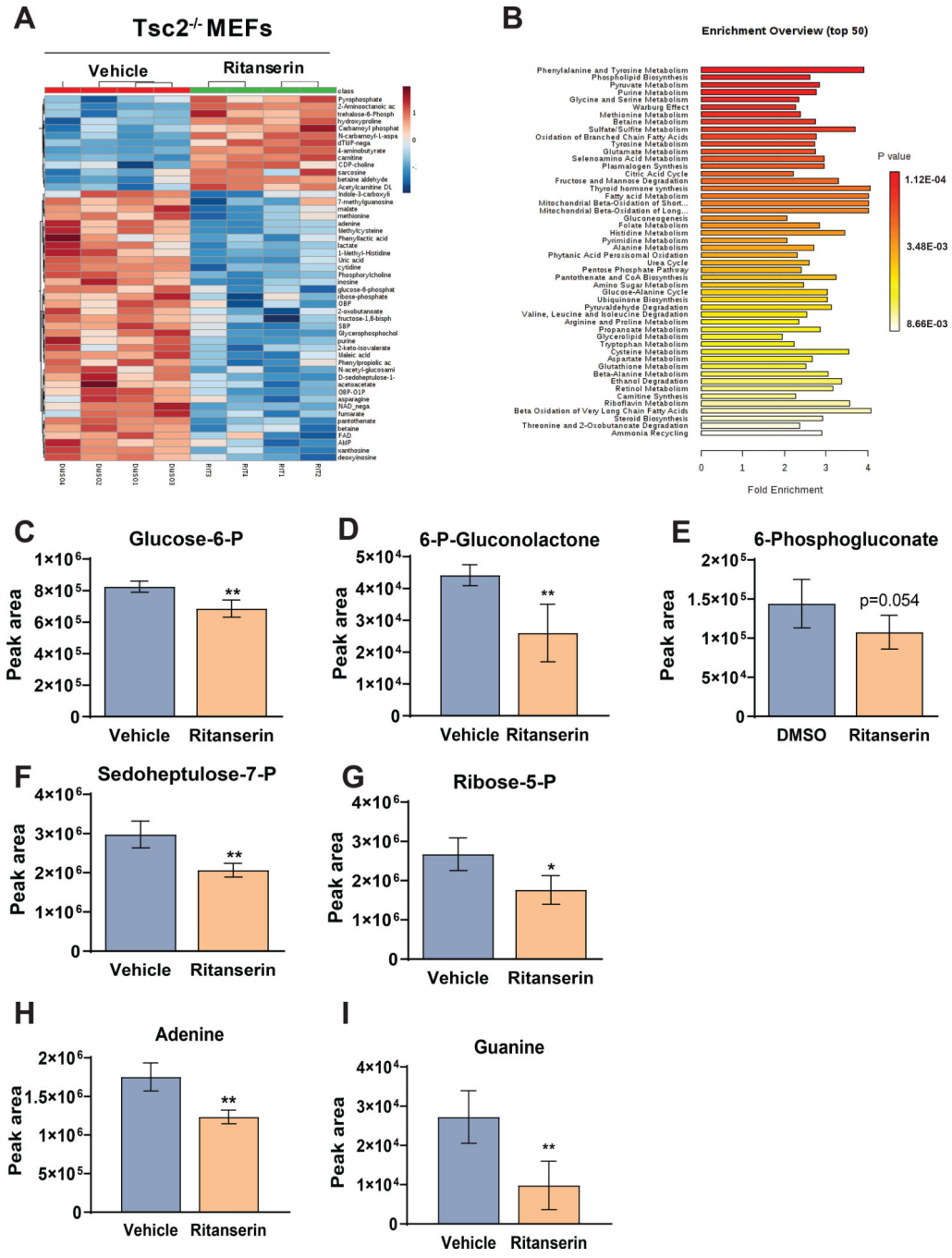

Figure 4. Ritanserin treatment rewires purine metabolism in Tsc2-deficient cells.

(A) Hierarchical clustering and heat map showing the top 50 differential metabolites in ritanserin treated Tsc2$^{-/-}$ MEFs. **(B)** Metabolite Set Enrichment Analysis (MSEA) identified differentially regulated metabolic pathways with FDR q<0.05. **(C-G)** LC/MS reveals that pentose phosphate pathway intermediate metabolites are decreased upon ritanserin treatment (10uM; 16 hours). **(H-I)** Purines adenosine and guanine are decreased following ritanserin treatment. Data presented as mean ± SD of four biological replicates. Statistical significance

was assessed using t-test with FDR correction ($q<0.05$) and *$p<0.05$, **$p<0.01$, ***$p<0.001$, ****$p<0.0001$.

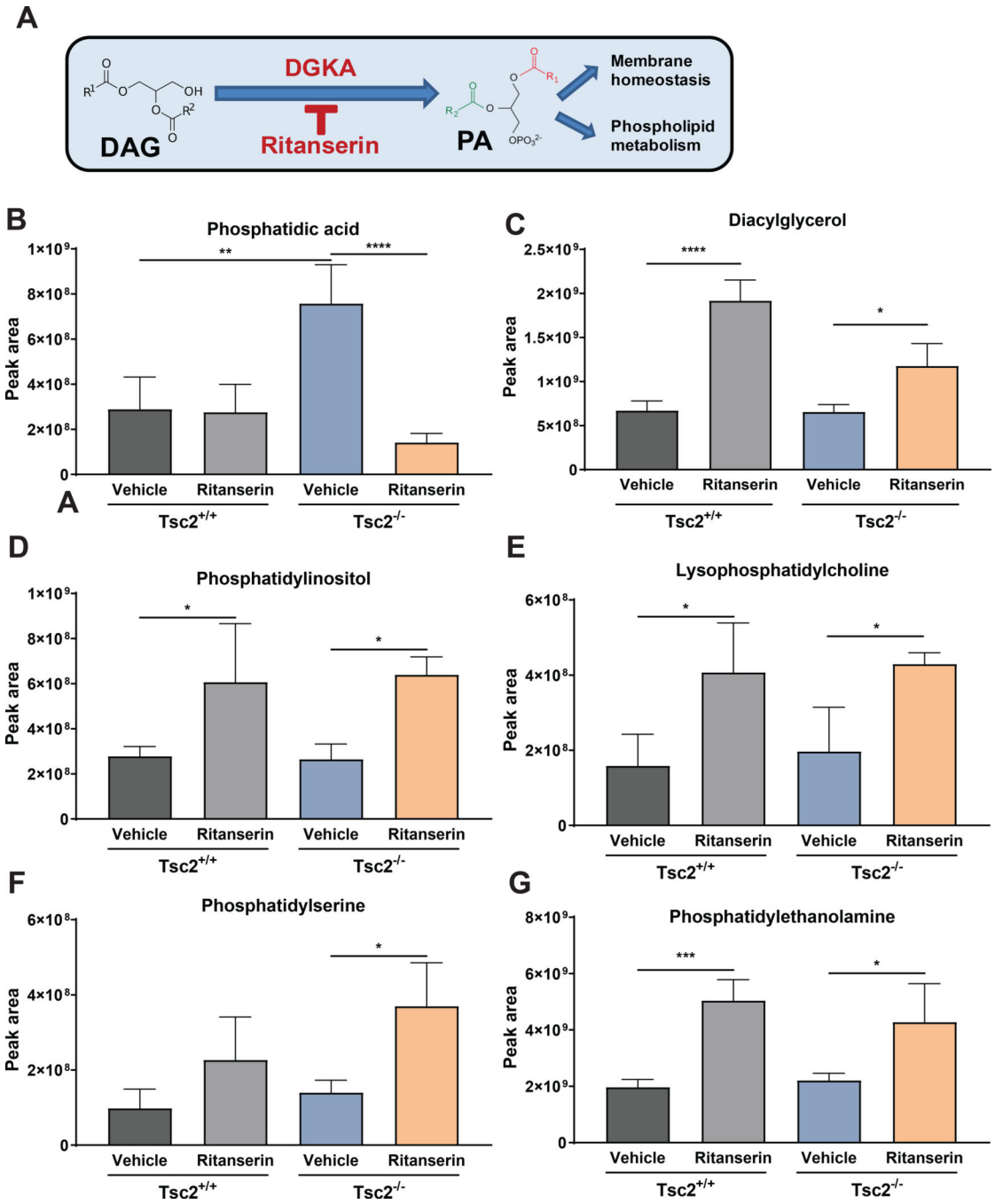

Figure 5. Ritanserin induces phospholipid reprogramming in Tsc2-deficient cells.

(A) Schematic representation of diacylglycerol metabolism to phosphatidic acid via DGKA. **(B)** Phosphatidic acid levels are elevated in $Tsc2^{-/-}$ MEFs compared to $Tsc2^{+/+}$ MEFs. Ritanserin treatment (10uM; 16 hours) decreases PA levels in $Tsc2^{-/-}$ MEFs but not in $Tsc2^{+/+}$ MEFs. **(C-G)** DGKA inhibition by ritanserin leads to accumulation of diacylglycerol and phospholipids PI, PC, PS and PE similarly in $Tsc2^{-/-}$ MEFs and in $Tsc2^{+/+}$ MEFs. Data presented as mean ± SD of the sum of each lipid species from three

biological replicates. Statistical significance was assessed using t-test with FDR correction ($q<0.05$) and *$p<0.05$, **$p<0.01$, ***$p<0.001$, ****$p<0.0001$.

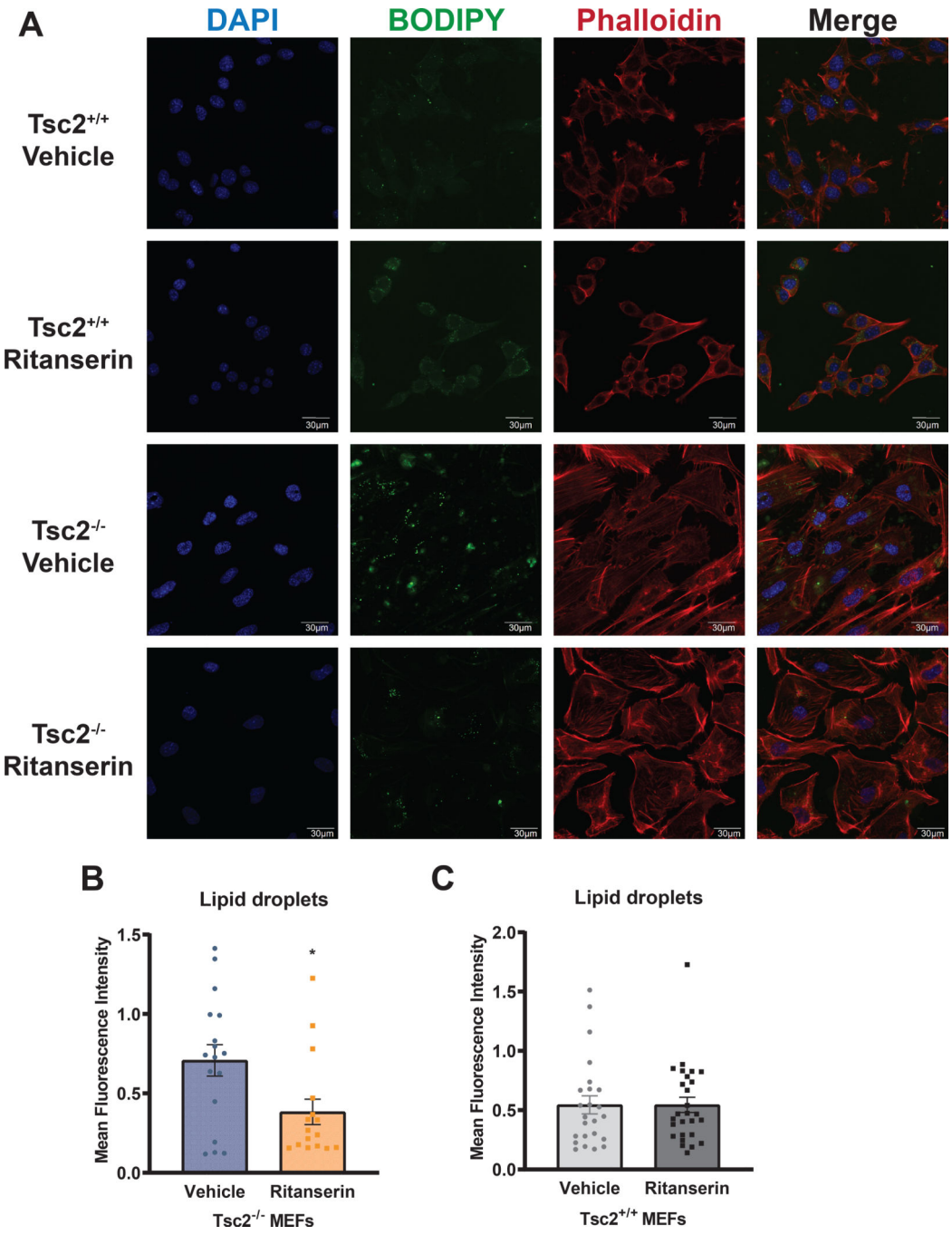

Figure 6. Lipid droplet formation in Tsc2-deficient cells is mediated via DGKA.

(A) Representative images from $Tsc2^{+/+}$ and $Tsc2^{-/-}$ MEFs treated with vehicle control (DMSO) or ritanserin (10uM; 16 hours). Lipid droplet content (10uM BODIPY 493/500) was increased in $Tsc2^{-/-}$ MEFs compared to $Tsc2^{+/+}$ MEFs. F-actin was visualized using Phalloidin 578/600 (10uM). **(B-C)** Quantification of lipid droplets in $Tsc2^{-/-}$ and $Tsc2^{+/+}$ MEFs following ritanserin treatment using CellProfiler (Broad Institute). Fluorescence intensity is represented as mean +/− standard deviation from >20 cells per condition. Statistical significance was assessed using unpaired t-test with *$p < 0.05$.

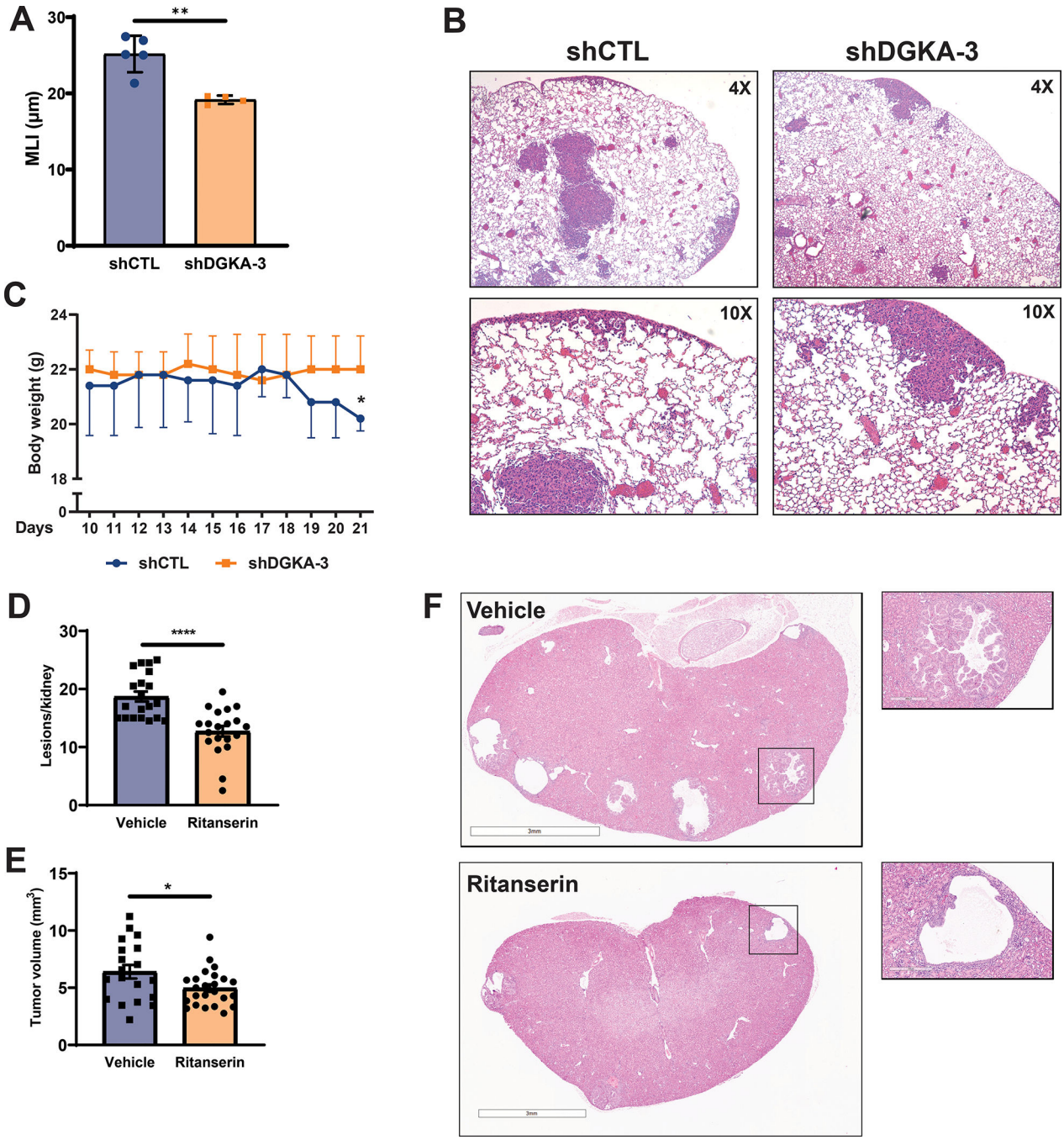

Figure 7. Therapeutic targeting of DGKA decreases alveolar airspace enlargement in a preclinical model of LAM and prevents cyst formation in a model of TSC.

(A) Mean linear intercept quantification shows that DGKA downregulation decreases the alveolar airspace in lung sections from NCr mice injected with 3 million shDGKA (n=4 mice) or shCTL (n=5 mice) TTJ cells. **(B)** H&E stained lung sections from mice injected with shCTL or shDGKA TTJ cells. **(C)** Body weight of mice injected with shCTL TTJ cells decreased by 20% 19 days after injection. **(D, E)** Ritanserin (20mg/kg/daily) reduced the number of lesions and overall tumor burden of $Tsc2^{+/-}$ A/J mice after 30 days of treatment.

(F) H&E stained kidney sections from mice treated with vehicle (upper panels) and ritanserin (lower panels). Data are represented as mean +/− standard deviation and statistical significance was assessed using unpaired t-test with *$p<0.05$.